








Reveling the Structural, Electric, and High-Frequency Dielectric Properties of Residue Doped- CaWO_4 Flexible Multilayer Ceramic Sheets

N. L. C. Siqueira^{a*} , H. P. Alves^b , P. H. Chibério^a , A. L. Silva^c , W. Acchar^{a,c} ,
F. Bohn^c , M. A. Correa^{a,c} 

^aUniversidade Federal do Rio Grande do Norte, Programa de Pós-Graduação em Ciência e Engenharia de Materiais, 59078-970, Natal, RN, Brasil.

^bUniversidade Federal da Paraíba, Programa de Pós-Graduação em Ciência e Engenharia de Materiais, 58051-900, João Pessoa, PB, Brasil.

^cUniversidade Federal do Rio Grande do Norte, Departamento de Física, 59078-970, Natal, RN, Brasil.

Received: November 18, 2024; Revised: January 23, 2025; Accepted: February 04, 2025

The mineralization process to reach Tungsten (W) involves several steps to reduce the impurities (residues), which makes the process more expensive. However, it is possible to explore the pure scheelite (CaWO_4) and residue doped- CaWO_4 on flexible sheets using the Tape Casting technique. In particular, the high frequency dielectric properties of flexible multilayers have an increased appeal in the electronics industry. In this study, we present a systematic investigation of structural, morphological, electrical and high-frequency dielectric properties of flexible ceramics sheet multilayers composed of pure CaWO_4 and residue-doped CaWO_4 . Our findings demonstrate that the dielectric constant has a small dependence on the residue amount, but a remarkable modification in the dielectric constant as the number of layers increases. Here we achieved a 34% increase in the dielectric constant for pure CaWO_4 flexible ceramic sheets when the number of layers increased from 1 to 3.

Keywords: flexible ceramic sheet, tape casting, scheelite, CaWO_4 .

1. Introduction

The dielectric constant (ϵ) is a fundamental physical parameter that characterizes the ability of a material to respond to electromagnetic waves or an applied electric field, influencing its performance across a wide range of applications¹. Ceramic films, sheets, and dielectric multilayers have emerged as critical components in modern electronics, with their most prevalent applications being in capacitors^{2,3}, energy storage systems⁴, piezoelectric devices⁵. More recently, these materials have been explored for their potential in advanced technologies, including devices designed for 5G communication systems^{6,7}. The combination of ceramics with polymers has attracted considerable interest in the field of dielectric applications, as it synergistically integrates the flexibility and cost-efficiency of polymers with the superior dielectric properties of ceramics⁸. Nevertheless, most studies investigating the dielectric properties of these materials have predominantly focused on low-frequency regimes (MHz), highlighting the pressing need for further exploration of their behavior and potential applications in high-frequency domains (GHz)⁹.

Simultaneously, the depletion of fossil fuel reserves and the growing demand for sustainable energy solutions have underscored the necessity of developing renewable energy technologies and efficient energy storage systems¹⁰. In this context, advanced materials, such as tungsten-based compounds, have garnered significant attention for their exceptional

physicochemical and electrochemical properties. These materials have found applications in various technological domains, including solar cells, supercapacitors, batteries, smart windows, and sensors¹¹. The convergence of these advancements highlights the critical role of innovative material systems, such as ceramic-polymer composites and tungsten-based materials, in addressing the challenges of modern energy and electronic systems while paving the way for sustainable technological progress.

Within this context, Scheelite (CaWO_4) stands as a primary ore for tungsten extraction, a metal prized for its elevated melting point and exceptional hardness. Tungsten finds widespread application in the production of robust alloys, notably tungsten carbide, which serves pivotal roles in the crafting of cutting tools, drill bits, and various high-wear implements. It's worth noting that tungsten is not naturally encountered in its metallic state; rather, it is commonly found in association with other elements. The two predominant mineral forms in which tungsten occurs in nature are Wolframite and Scheelite¹².

Nevertheless, the mining of tungsten comes with environmental challenges. Tungsten mining can lead to environmental consequences, including soil and air pollution. Additionally, noise and visual disturbances arise from mining operations such as crushing and blasting. These environmental impacts underscore the importance of adopting sustainable practices and mitigating measures in extracting and processing tungsten resources¹³. Notably, 99%

*e-mail: nivialsiqueira@gmail.com

of the scheelite beneficiation process generates residues, with only 0.8% of the ore destined for commercial use. In recent years, several authors have explored the utilization of mining residues such as scheelite residue within the construction sector. Their aim is twofold: to reduce production costs by employing such by-products as raw materials and to reduce environmental impacts associated with the uncontrolled disposal of these residues. The results have proven promising, as the inclusion of scheelite residue in formulations not only fulfills the objectives but also enhances the properties of the resulting materials^{14,15}

From an electrical property perspective, scheelite exhibits remarkable potential application as a ceramic electrolyte for solid oxide fuel cells¹⁶⁻¹⁸. However, the electrical features, including dielectric properties, strongly depend on the material concentration, including impurities originating from the mining process. Moreover, the search for ceramic materials that are easy to mold on a given surface brings to light the need to explore the cited properties of flexible systems. Tape Casting seems to be a promising technique to produce scheelite flexible ceramics sheets for electrical and dielectric applications within this context. The process primarily involves creating slurry with pseudoplastic behavior by blending ceramic powders, solvent, binder, plasticizer, and other additives, and the slurry is subsequently cast onto a carrier substrate, with the shape and thickness determined by a doctor blade. The green sheets produced can undergo further processes, such as cutting, lamination, and thermal treatment^{19,20}

However, there was an absence of studies in which the dielectric properties of CaWO_4 at high frequencies are explored for future technological applications. This high-frequency property is fundamental in integrating ceramic sheets as the base of integrated electronic devices, mainly for capacitors, telecommunications and energy storage systems. Motivated by this challenge, we investigated the structural, electrical, and dielectric properties of a heterostructure comprising concentrated scheelite (CS) and residual scheelite (RS) in multilayer ceramic sheets. This study lays the foundation for potential applications in the dynamic realm of electronics. Our findings demonstrate the dependence of electric and dielectric properties considering the purity of the flexible heterostructure ceramics sheet composed of scheelite material. Moreover, we demonstrate that the scheelite residue can be added to the flexible ceramic sheets for high-frequency technological applications. The multilayer structure demonstrates an exciting route to tune the dielectric constant of flexible ceramic sheets.

2. Experimental Procedure

To produce the ceramics sheets was considered concentrated scheelite (CS) (WO_3 -rich material) and the scheelite residue (SR) (CaO-rich material) from Brejui Mine, Brazil. In Particular, northeast of Brazil, more specifically the state of Rio Grande do Norte, has a strong mineral activity in scheelite production. This issue has been explored by distinct research groups with the intention of promoting a lower environmental impact from waste during production.

For this purpose, the scheelite powders were dried in an oven at 120 °C and sieved to < 74 μm (200 mesh).

We prepared flexible heterostructure ceramic sheets with compositions ranging from 0 to 100 wt.% of 25 wt.% increments. The sheets were named 100C, 75C, 50C, 25C, 100R, corresponding to 100 wt.% CS, 75 wt.% CS and 25 wt.% SR, 50 wt.% CS and 50 wt.% SR, 25 wt.% CS, and 75 wt.% SR, 100 wt.% SR, respectively. The mixing of concentrated scheelite and the scheelite residue occurred similarly to the work carried out by Alves et al.²¹. The suspensions were prepared in two stages. First, distilled water, ethyl alcohol, triton X-114, and ceramic powder were mixed in a ball mill for 24 h. Subsequently, 16.6% hydrolyzed Poly (Vinyl Alcohol) (PVA), glycerol, coconut diethanolamine, and antifoam were added to the mixture and homogenized for 24 h. The sequence used in adding the suspension components was carefully carried out to avoid adsorption competition between the dispersant and binder on the surface of the particles²². The compositions used to prepare ceramic suspensions are presented in Table 1.

The suspensions were cast using a Mistier TCC-1200 tape caster (Tape Casting Warehouse, Inc.) at room temperature, with a speed of 20.2 cm/min. The leveling blade was adjusted to 650 μm and the ceramic sheets were dried in the equipment at room temperature and controlled atmosphere for 24 h.

The chemical composition of CS and RS powders was analyzed through X-ray fluorescence spectroscopy (XRF) to determine the chemical composition using a Shimadzu EDX-700 equipment. Suspension viscosity measurements were acquired using a Haake Viscotester-Thermo Fischer Scientific model viscometer with cone/plate geometry at room temperature and with shear stress between 0 and 1000 s^{-1} . Thermogravimetric analysis (TGA) of the ceramic sheets was carried out in a Shimadzu DTG-60 analyzer in an argon atmosphere, with a flow rate of 50 mL/min and a temperature ranging from 25 °C to 600 °C with a heating rate of 5 °C/min. The structural properties were done by X-ray diffraction measurements, a Rigaku Miniflex II diffractometer with $\text{Cu-K}\alpha$ radiation, and $\theta - 2\theta$ Bragg-Brentano geometry was used. Rietveld refinement of the XRD data was performed, thus providing information on the crystalline phase content, lattice parameters, and quality factors. Moreover, Scanning Electron Microscope (SEM) with field emission gun (SEM-FEG) images were observed using the Zeiss Auriga 40 model. The electrical properties (electrical resistivity) were verified by using I vs. V curves with a 4-point configuration. For this purpose, a Keithley 238 source was used, and the measurements were realized at room temperature.

High-frequency dielectric characterizations of the ceramic sheets were obtained from multilayer sheets. In particular, the multilayer allows the improvement of the dielectric constant since this property is strongly dependent on the studied thicknesses. Here, we provide a systematic study in multilayer composed of 1, 2, and 3 sheets. The dielectric measurements were performed using an Agilent E4991A RF impedance/material analyzer with a dielectric measurement module at room

temperature. In particular, we considered a frequency range between 0.15 GHz and 1.5 GHz for this technique. The calibration process was performed with a Teflon plate 0.77 mm thick and a standard dielectric constant of 2.1. In this case, the real and imaginary ϵ' components of the electrical permittivity were acquired simultaneously in the experiment. The dielectric constant corresponds to the real component of the permittivity, and the dielectric loss is defined as ϵ''/ϵ' . It is important to point out that all the structural, morphologic, electric, and dielectric properties were performed at room temperature. This feature is important to verify the effective potential of technological applications of the studied material.

3. Results and Discussion

The chemical compositions measured through XRF are summarized in Table 2. In particular, the table presents the wt.% for the CS and SR powder used to produce the heterostructure flexible sheets. From the results, we observed that the CS is composed predominantly of WO₃, with a content of 68.30 wt.%, followed by CaO, with 14.30 wt.%. Fe₂O₃, MoO₃, SO₃, Al₂O₃, P₂O₅, and BaO oxides represent about 16.20 wt.% of CS. This result agrees with the literature for similar systems^{23,24}.

Regarding the RS, we noticed a high amount of CaO in the chemical composition, representing 47.90 wt.%, followed by SiO₂ (22.3 wt.%), Fe₂O₃ (15.6 wt.%), and Al₂O₃ (5.80 wt.%), and smaller amounts of MgO (2.3 wt.%), WO₃ (1.9 wt.%), SrO (1.1 wt.%) and MnO (0.9 wt.%).

We verified a sharp decline in the amount of WO₃ present in the RS compared to the CS, confirming the efficiency of the mineral beneficiation process^{25,26}.

Figure 1(a) depicts the viscosity curves as a function of the shear rate for the five ceramic suspensions. The suspensions show non-Newtonian fluid behavior, with a decrease in viscosity as the shear rate increased, characterizing pseudoplastic behavior, a fundamental issue to produce a homogenous flexible sheet^{27,28}. Figure 1(b) depicts the Weight loss as a function of the temperature (TGA analysis). The results show a similar trend for all studied materials with a total weight loss of approximately 22.44 wt.%. The first weight loss occurs between temperatures of 106 °C and 248 °C with 2.18 wt.%, attributed to the elimination of water molecules²⁹. The second and third weight loss occurs between the temperatures of 248 °C – 372 °C and 372 °C – 472 °C with 15.76 wt.% and 4.50 wt.%, respectively. These losses are associated with the decomposition of organic constituents in the ceramic sheets^{30,31}.

The refined XRD patterns verify the structural properties of the pure ceramic sheets and those doped with scheelite residue, as seen in Figure 2. The diffraction peaks are related to the phases: CaWO₄ (ICSD-15869, tetragonal symmetry and space group I41/a: 1)³², CaCO₃ (ICSD-40113, trigonal symmetry and space group R-3c: H)³³ and MnSiO₃ (ICSD-34343, triclinic symmetry and space group P-1)³⁴. The lattice parameters, phase quantifications, and quality factors (R_{wp} , R_{exp} , and χ^2) are shown in Table 3.

Table 1. Parameters used in the two-step preparation of ceramic suspension.

Steps	Material	Role	wt.%
1°	Distilled water	Solvent	25.0
	Ethyl alcohol	Solvent	13.0
	Triton x-114	Dispersant	2.0
	Ceramic powder	Powder	29.0
	Polyvinyl alcohol (PVA)*	Binder	25.0
2°	Glycerol	Plasticizer	4.5
	Coconut diethanolamide	Surfactant	0.5
	Antifoam A	Antifoam	1.0

* Weigher PVA powder was dissolved in distilled water at 60 °C and the solution was stirred for 1 hour to provide PVA solution 16 (%w/v).

Table 2. XRF results for the CS powder and RS powder.

Concentrated scheelite (CS)		Residue scheelite (RS)	
Oxides	Content (wt.%)	Oxides	Content (wt.%)
WO ₃	68.3	CaO	47.9
CaO	14.3	SiO ₂	22.3
Fe ₂ O ₃	5.2	Fe ₂ O ₃	15.6
MoO ₃	3.9	Al ₂ O ₃	5.8
SO ₃	3.9	MgO	2.3
Al ₂ O ₃	1.5	WO ₃	1.9
P ₂ O ₅	1.2	SrO	1.1
BaO	0.5	MnO	0.9

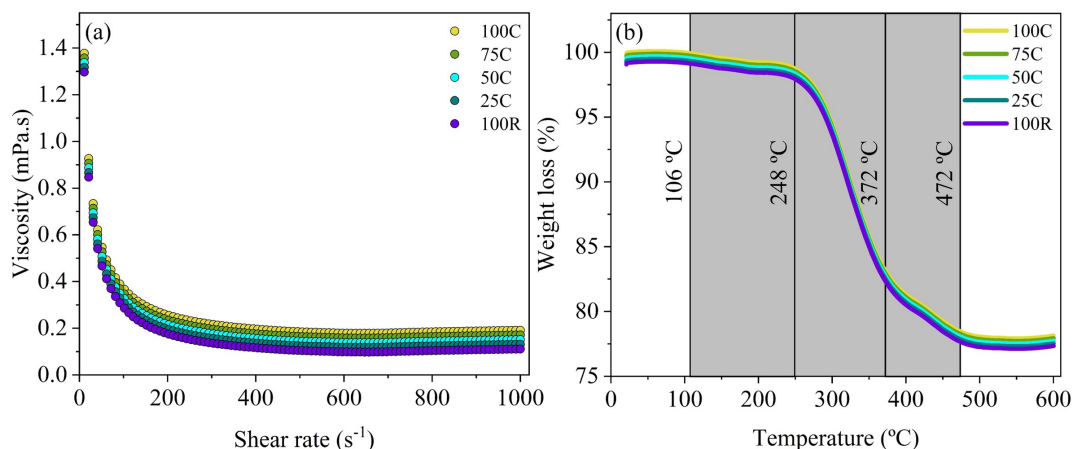


Figure 1. (A) Viscosity as a function of shear rate for the studied samples. (B) TGA behavior of 100C, 75C, 50C, 25C and 100R ceramic sheets.

Through the quality factors, we verified a good agreement between the values calculated via refinement and the experimental values via XRD. Furthermore, we observed that the 100C sheet only presents the $CaWO_4$ phase. On the other hand, the sheet containing only the scheelite residue (100R) exhibits $CaCO_3$ and $MnSiO_3$ phases. These results agree with the data reported in FRX. According to the Rietveld refinement, we noticed an increase in the $CaCO_3$ phase with increasing SR content, where the diffraction position of the (104) plane located at $2\theta = 29.28$ for $CaCO_3$ presents greater intensity in the 25C sheet³⁵. Also, we noticed in 75C, 50C, and 25C sheets that the main $CaWO_4$ peak is located at $2\theta = 28.72$, corresponding to the crystalline plane (112)³⁶.

The morphological aspects of the flexible ceramic sheets are shown in Figure 3(a-e). From the images, it is possible to verify that the powder particles are dispersed in the polymeric matrix. Also, it is possible to observe particles with varied sizes and irregular geometries since, after the dispersion of the scheelite powder in the polymeric matrix, these particles tend to agglomerate to minimize the surface energy. Our results demonstrate the efficiency of the tape-casting technique in obtaining the proposed morphology, offering a versatile means to control chemical and physical properties. This includes the manipulation of parameters like electrical and dielectric constants which will be further discussed.

The electric properties, measured by using the 4-point technique, are depicted in Figure 4. Considering the high electrical resistivity of the flexible ceramic sheets, the low current range was considered. Figure 4(a) depicts the electric I vs. V curves for all studied flexible ceramic sheets. From the curves, it is evident a slight modification of the electric properties with the CS amount increases. However, all the samples present similar behaviors. It is important to point out, that the present characterization has the contribution of the organic components of the flexible ceramic sheets, which contribute to the increase of the electrical resistivity of the sheets. Figure 4(b) shows the electric resistivity of the studied sheets as a function of the CS amount. From the

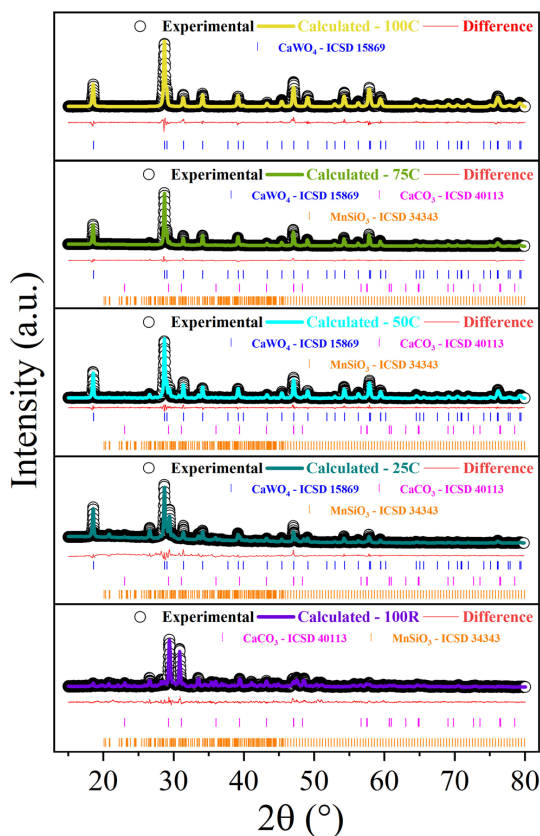


Figure 2. Refined XRD patterns of the ceramic sheets.

results, we observe a slight increase in the electric resistivity for the 100C flexible sheet. This result is expected since we verified a considerable increase in the WO_3 amount for the 100C flexible sheet, which agrees with the structural results presented before.

The changes in the electric properties modify the charge mobility in the proposed heterostructure. Consequently,

Table 3. Parameters obtained from the Rietveld refinement.

Sample	Phase	wt. (%)	Latt. Par. (Å)	Agreement factors		
				R _{wp} (%)	R _{exp} (%)	χ ²
100C	CaWO ₄	100	a = b = 5.2464(9) c = 11.3844(7)	16.06	9.87	1.62
75C	CaWO ₄	75.49	a = b = 5.2465(6) c = 11.3839(9)	14.85	10.95	1.54
	CaCO ₃	17.92	a = b = 4.9878(4) c = 17.0609(1)			
	MnSiO ₃	6.59	a = 6.7193(6) b = 7.6015(3) c = 17.4508(8)			
	CaWO ₄	41.31	a = b = 5.2444(2) c = 11.3786(8)			
50C	CaCO ₃	31.08	a = b = 4.9851(9) c = 17.0668(8)	13.90	10.53	1.32
	MnSiO ₃	17.61	a = 6.7352(3) b = 7.6385(2) c = 17.4320(9)			
	CaWO ₄	25.76	a = b = 5.2459(1) c = 11.3824(9)			
	CaCO ₃	47.36	a = b = 4.9870 (6) c = 17.0467(7)			
25C	MnSiO ₃	26.88	a = 6.6554(1) b = 7.6082(2) c = 17.3807(6)	16.21	10.08	1.41
	CaCO ₃	60.36	a = b = 4.9860(5) c = 17.0456(4)			
	CaCO ₃	60.36	a = b = 4.9860(5) c = 17.0456(4)			
	MnSiO ₃	39.64	a = 6.6718(7) b = 7.6342(6) c = 17.5414(9)			
100R	MnSiO ₃	39.64	a = 6.6718(7) b = 7.6342(6) c = 17.5414(9)	18.88	10.03	1.88

these modifications can reflect on the dynamics of electric response. To verify this issue, we provide a systematic study of the dielectric measurements at a high-frequency regime. Charge dynamics, measured through dielectric measurements can bring interesting information about the applicability of these materials for future devices. Based on this feature, Figure 5 shows the dielectric constant measured at a high-frequency regime (0.1 up to 1.5 GHz), at room temperature. It is important to point out that, for this frequency regime the main mechanism acting on the dielectric constant modification is the dipolar one. This mechanism leads to a considerable reduction in the dielectric constant, in comparison with that one verified at a low-frequency regime (tens of MHz).

Moreover, in our case, it is important to mention the presence of organic material in the flexible ceramic sheets, which may lead to a reduction of the dielectric constant of

the heterostructure. However, all the studied flexible ceramic sheets present the very same organic material, which leads to a similar contribution, regardless of the CS concentration. This feature allows us to realize a comparison between the dielectric constants verified for our ceramic sheets.

Figure 5(a) shows the dielectric constant for a single layer of flexible ceramics sheet for distinct concentrate Scheelite amount. With concern to the CS we observe a weak modification on the dielectric constant. It is remarkable the similarity of the dielectric constant between the 100R and 100C flexible sheets. This feature is directly connected with the morphology of the samples and the dielectric constant of the WO₃, CaO, and SiO₂. For low CS values the CaO and SiO₂ dominate de material concentration of the alloy (see XRF results). Consequently, the dielectric constant of the flexible ceramic sheets should reflect the characteristics of the CaO and SiO₂³⁷.

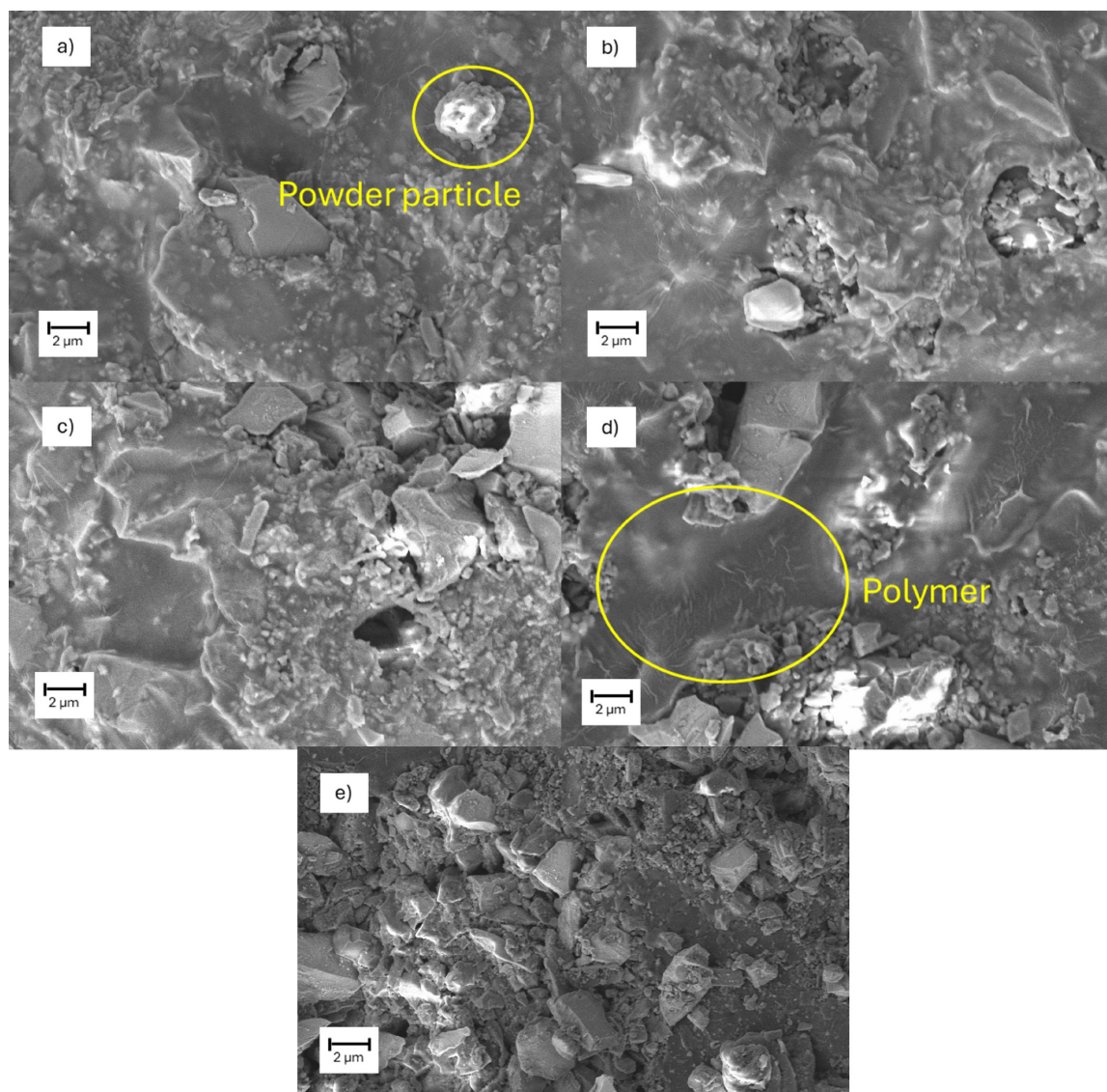


Figure 3. SEM images for (a) 100R, (b) 25C, (c) 50C, (d) 75C and (e) 100C.

To enhance the dielectric constant by reducing the energy loss, we increase the number of layers from 1 to 3. The results show that with the increase of the flexible ceramic layers, we observe a remarkable increase in the dielectric constant, irrespective of the concentrate Scheelite amount. This feature is expected, due to the increase of the thicknesses, of the analyzed material as well as with the biggest material contributing to the electric polarization. These values are consistent with that one observed in the literature, which verified a value of 7.2 for the CaWO_4 for measurements realized at a similar frequency regime³⁸. Considering the Loss factor, depicted in Figure 6, we verified a low loss for all studied material. However, these values increase as the layers rise. As expected, with an increase in the thickness of the flexible ceramic sheets, the overall volume through which the electric field extends also increases. This larger volume provides more pathways for the dissipation of electrical

energy, leading to higher dielectric losses. Thicker materials exhibit a higher likelihood of internal interfaces, defects, or variations in morphology as present in SEM results, Figure 3. These factors contribute to additional loss mechanisms, such as interfacial polarization, resulting in increased dielectric losses. Considering the frequency-dependent nature of dielectric losses, thicker materials exhibit more significant losses at higher frequencies due to the limited mobility of the charge carrier.

Figure 7 shows the mean values of the dielectric constant calculated between 0.2 and 1.5 GHz, as a function of the concentrate scheelite amount. This representation allows us to verify the evolution of the dielectric constant as a function of the number of flexible layers on the multilayer. From the results, we observe a tiny modification in the dielectric constant as the CS increases. However, the remarkable results are verified by comparing the means dielectric constant as a

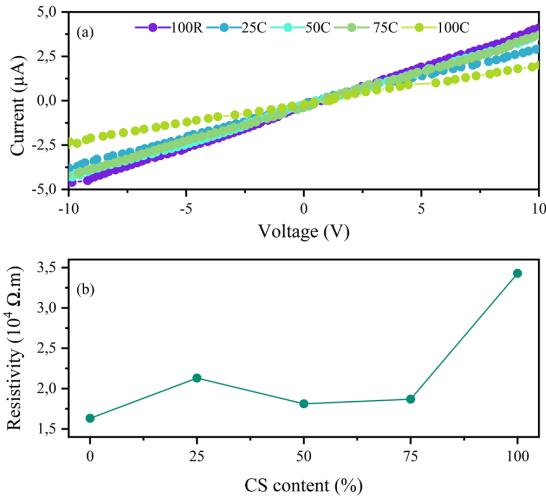


Figure 4. (a) I vs. V curves for the studied flexible ceramic sheets (b) electric resistivity as a function of the scheelite amount. Electric resistivity as a function of CS concentration on the flexible ceramic sheets. The inset depicts the I vs. V curves for the studied flexible sheets.

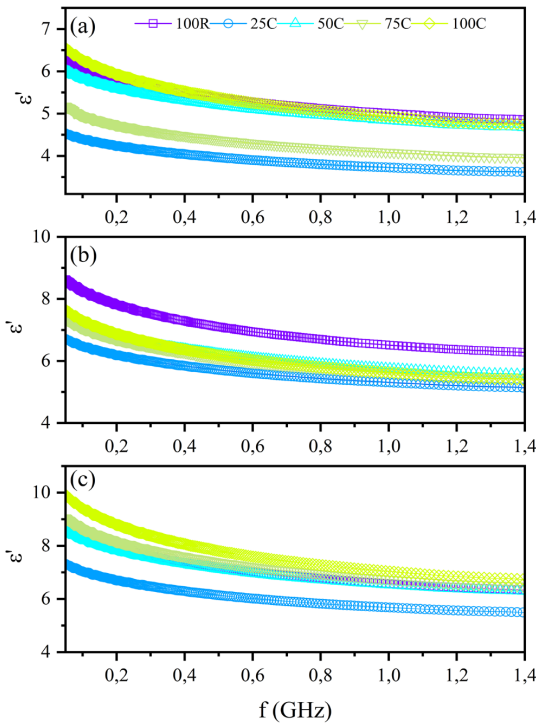


Figure 5. Dielectric constant as a function of frequency for the studied samples. (a) Dielectric constant (ϵ') for in a single flexible layer. (b) similar plot for two flexible layers (c) three flexible layers.

function of layer on the system. The considerable increase in the dielectric constant for the multilayer is evident. Considering the 100C sheet, in which we have pure CS the dielectric constant increases from 6.2 for a single flexible layer to 10.2 for the multilayer composed of three sheets.

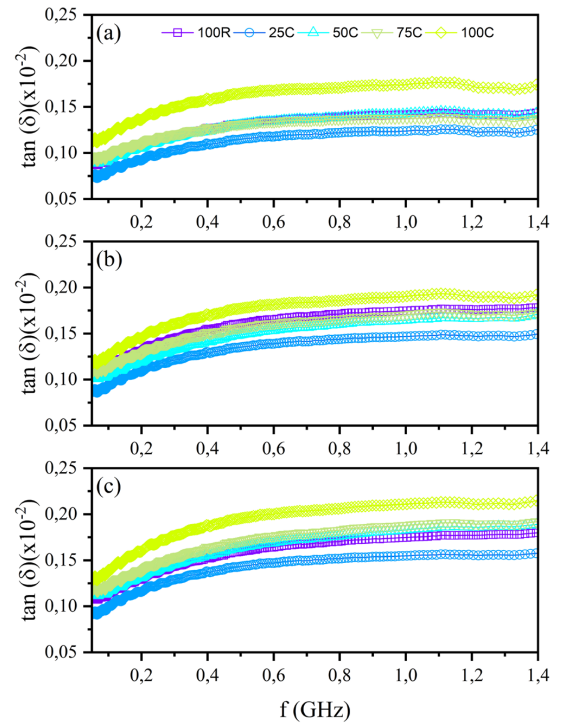


Figure 6. Loss factor as a function of frequency for the studied samples. (a) Loss factor ($\tan(\delta)$) for in a single flexible layer (b) similar plot for two flexible layers (c) three flexible layers.

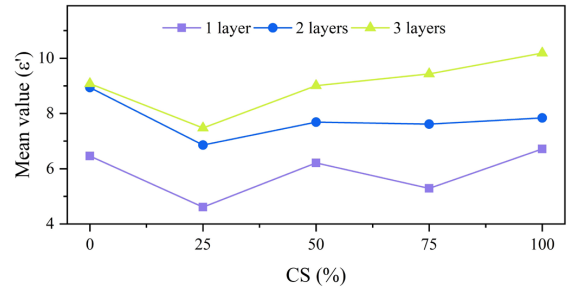


Figure 7. Means values of ϵ' calculated between 0.2 and 1.5 GHz as a function of the CS content, for the distinct number of flexible layers.

This modification characterizes an increase of around 34% on the dielectric constant. These results open a new route to tune the dielectric constant of these flexible ceramic sheets for distinct technological applications.

4. Conclusion

This study systematically examined the structural, electrical, and dielectric properties in the high-frequency regime of multilayer ceramic sheets composed of Concentrated Scheelite (CS) and Scheelite Residue (SR) produced by the Tape Casting method. The incorporation of SR, often regarded as a by-product with no commercial value, is shown as a viable alternative for reducing production costs

while mitigating the environmental impacts associated with tungsten mining. The dielectric properties of the sheets remained notably stable regardless of the incorporation of residue, highlighting the potential for integrating sustainable materials into production processes without compromising product functionality. One of the most significant findings of this research is the ability to tune the dielectric constant by incorporating multilayer structures. By adding flexible ceramic layers, the dielectric constant increased by 34%. This enhancement can be attributed to the combined effects of increased material thickness and greater polarization, underscoring the crucial role of multilayer configurations in optimizing dielectric performance.

Furthermore, the low dielectric losses observed across all samples point to the strong suitability of these materials for high-frequency applications, such as capacitors, telecommunications, and energy storage systems. This study not only advances our understanding of the properties of flexible ceramic sheets but also demonstrates a sustainable approach to utilizing mining residues. These findings pave the way for the development of high-performance and environmentally friendly materials for technology and advanced electronic systems.

5. Acknowledgments

This work was supported by Coordenação de Aperfeiçoamento de Pessoal de Nível Superior (CAPES) and Conselho Nacional de Desenvolvimento Científico e Tecnológico (CNPq). MAC acknowledges the support of the INCT of Spintronics and Advanced Magnetic Nanostructures (INCT-SpinNanoMag), CNPq 406836/2022-1.

Data Availability

Not applicable.

6. References

- Xie P, Shi Z, Feng M, Sun K, Liu Y, Yan K, et al. Recent advances in radio-frequency negative dielectric metamaterials by designing heterogeneous composites. *Adv Compos Hybrid Mater.* 2022;5(2):679-95. <http://doi.org/10.1007/s42114-022-00479-2>.
- Beak K, Choi M, Kim DH, Yu Y, Theerthagiri J, Al-Mohaimed AM, et al. Silane-treated BaTiO₃ ceramic powders for multilayer ceramic capacitor with enhanced dielectric properties. *Chemosphere.* 2022;286:131734. <http://doi.org/10.1016/j.chemosphere.2021.131734>.
- Feng M, Feng Y, Zhang T, Li J, Chen Q, Chi Q, et al. Recent advances in multilayer-structure dielectrics for energy storage application. *Adv Sci.* 2021;8(23):2102221. <http://doi.org/10.1002/advs.202102221>.
- Pattipaka S, Lim Y, Son YH, Bae YM, Peddigari M, Hwang G-T. Ceramic-based dielectric materials for energy storage capacitor applications. *Materials (Basel).* 2024;17(10):2277. <http://doi.org/10.3390/ma17102277>.
- Habib M, Lantgios I, Hornbostel K. A review of ceramic, polymer and composite piezoelectric materials. *J Phys D Appl Phys.* 2022;55(42):423002. <http://doi.org/10.1088/1361-6463/ac8687>.
- Shehbaz M, Du C, Li R, Wang W, Hazaa Alzakree AR, Yao X-G, et al. Millimeter wave dielectric resonator antenna using high quality factor temperature stable dielectric ceramic composite K18 for 5G applications. *ACS Appl Electron Mater.* 2024;acsaelm.4c00995. <http://doi.org/10.1021/acsaelm.4c00995>.
- Li H, Wei P, Wang Y, Zhu Q, Wang X, Gao W, et al. High-frequency 5G substrate: low dielectric biphenyl polyimide with low CTE and high thermal stability. *Mater Today Adv.* 2024;23:100514. <http://doi.org/10.1016/j.mtadv.2024.100514>.
- Palani Velayuda Shanmugasundram HP, Jayamani E, Soon KH. A comprehensive review on dielectric composites: classification of dielectric composites. *Renew Sustain Energy Rev.* 2022;157:112075. <http://doi.org/10.1016/j.rser.2022.112075>.
- Kang Z, Ke S, Yin C, Wang W, Zheng S, Sun X, et al. Dielectric constant measurements of sweep frequency and its effect from 20 MHz to 1000 MHz. *J Petrol Sci Eng.* 2018;166:602-10. <http://doi.org/10.1016/j.petrol.2018.03.093>.
- Holechek JL, Geli HME, Sawalhah MN, Valdez R. A global assessment: can renewable energy replace fossil fuels by 2050? *Sustainability.* 2022;14(8):4792. <http://doi.org/10.3390/su14084792>.
- Shinde PA, Jun SC. Review on recent progress in the development of tungsten oxide based electrodes for electrochemical energy storage. *ChemSusChem.* 2020;13(1):11-38. <http://doi.org/10.1002/cssc.201902071>.
- Brown T, Pitfield P. Tungsten. In: Gunn G, editor. *Critical metals handbook*. Hoboken: Wiley; 2014. p. 385-413. <https://doi.org/10.1002/9781118755341.ch16>.
- Zheng X, Qiu S, Zhou B, Li Q, Chen M. Leaching of heavy metals from tungsten mining tailings: a case study based on static and kinetic leaching tests. *Environ Pollut.* 2024;342:123055. <http://doi.org/10.1016/j.envpol.2023.123055>.
- Souza MM, Anjos MAS, Sá MVVA. Using scheelite residue and rice husk ash to manufacture lightweight aggregates. *Constr Build Mater.* 2021;270:121845. <http://doi.org/10.1016/j.conbuildmat.2020.121845>.
- Durante Ingunza MP, dos Santos OF Jr, Gerab ATFSC. Potential use of sandy mining wastes as raw material in road construction. *Geotech Geol Eng.* 2020;38(5):5681-91. <http://doi.org/10.1007/s10706-020-01382-7>.
- Cheng J, He J. Electrical properties of scheelite structure ceramic electrolytes for solid oxide fuel cells. *Mater Lett.* 2017;209:525-7. <http://doi.org/10.1016/j.matlet.2017.08.094>.
- Cheng J, Liu C, Cao W, Qi M, Shao G. Synthesis and electrical properties of scheelite Ca_{1-x}SmxMoO_{4+δ} solid electrolyte ceramics. *Mater Res Bull.* 2011;46(2):185-9. <http://doi.org/10.1016/j.materresbull.2010.11.019>.
- Panda D, Hota SS, Choudhary RNP. Investigation of structural, topological, and electrical properties of scheelite strontium molybdate for electronic devices. *Inorg Chem Commun.* 2023;158:111501. <http://doi.org/10.1016/j.inoche.2023.111501>.
- Carter CB, Norton MG. *Ceramic materials science and engineering*. New York: Springer; 2013. <https://doi.org/10.1007/978-1-4614-3523-5>.
- Hotza D, Nishihora RK, Machado RAF, Geffroy P-M, Chartier T, Bernard S. Tape casting of preceramic polymers toward advanced ceramics: a review. *Int J Ceram Eng Sci.* 2019;1(1):21-41. <http://doi.org/10.1002/ces2.10009>.
- Alves HPA, Costa ACS, Carvalho BR, Bohn F, Correa MA, Acchar W. Incorporating graphene into a sintered ceramic tape: structural and magnetic properties of a zirconia-graphene composite. *Mater Lett.* 2020;270:127689. <http://doi.org/10.1016/j.matlet.2020.127689>.
- Nishihora RK, Rachadel PL, Quadri MGN, Hotza D. Manufacturing porous ceramic materials by tape casting: a review. *J Eur Ceram Soc.* 2018;38(4):988-1001. <http://doi.org/10.1016/j.jeurceramsoc.2017.11.047>.
- Bo F, Xianping L, Jinqing W, Pengcheng W. The flotation separation of scheelite from calcite using acidified sodium silicate as depressant. *Miner Eng.* 2015;80:45-9. <http://doi.org/10.1016/j.mineng.2015.06.017>.

24. Liu C, Feng Q, Zhang G, Chen W, Chen Y. Effect of depressants in the selective flotation of scheelite and calcite using oxidized paraffin soap as collector. *Int J Miner Process*. 2016;157:210-5. <http://doi.org/10.1016/j.minpro.2016.11.011>.
25. Medeiros AG, Gurgel MT, da Silva WG, de Oliveira MP, Ferreira RLS, de Lima FJN. Evaluation of the mechanical and durability properties of eco-efficient concretes produced with porcelain polishing and scheelite wastes. *Constr Build Mater*. 2021;296:123719. <http://doi.org/10.1016/j.conbuildmat.2021.123719>.
26. Almeida EP, Carreiro MEA, Rodrigues AM, Ferreira HS, Santana LNL, Menezes RR, et al. A new eco-friendly mass formulation based on industrial mining residues for the manufacture of ceramic tiles. *Ceram Int*. 2021;47(8):11340-8. <http://doi.org/10.1016/j.ceramint.2020.12.260>.
27. Alves HPA, Costa ACS, Correa MA, Bohn F, Della Pace RD, Acchar W. Structural, magnetic and electric properties of ZrO₂ tapes decorated with magnetic nanoparticles. *Ceram Int*. 2019;45(12):14500-4. <http://doi.org/10.1016/j.ceramint.2019.04.123>.
28. Costa ACS, Alves HPA, Correa MA, Bohn F, Acchar W. Iron oxide/PVA flexible magnetic tape engineered by microwave combustion and tape casting. *Mater Chem Phys*. 2019;232:1-5. <http://doi.org/10.1016/j.matchemphys.2019.04.027>.
29. Barros MD, Hotza D, Janssen R. Colloidal processing and characterization of TiO₂-MnO-doped alumina/alumina slurries and tapes. *Int J Ceram Eng Sci*. 2021;3(4):173-9. <https://doi.org/10.1002/ces2.10087>.
30. Correa MA, Araujo MR, Acchar W, Souza ALR, Melo AS, Bohn F. ZrO₂ tape as flexible substrate to artificially nanostructured materials. *Mater Lett*. 2017;196:69-73. <http://doi.org/10.1016/j.matlet.2017.03.027>.
31. Peres APS, Costa ACS, Bohn F, Correa MA, Acchar W, Paskocimas CA. Bi₄Ti₃O₁₂ multilayered ceramic tapes produced by aqueous tape casting and laminating process: structural and dielectric properties. *Ceram Int*. 2018;44(13):16062-5. <http://doi.org/10.1016/j.ceramint.2018.05.146>.
32. Wang S, Gao H, Sun G, Li Y, Wang Y, Liu H, et al. Structure characterization, optical and photoluminescence properties of scheelite-type CaWO₄ nanophosphors: effects of calcination temperature and carbon skeleton. *Opt Mater (Amst)*. 2020;99:109562. <http://doi.org/10.1016/j.optmat.2019.109562>.
33. Tang Z, Cheng G, Chen Y, Yu X, Wang H. Characteristics evaluation of calcium carbonate particles modified by surface functionalization. *Adv Powder Technol*. 2014;25(5):1618-23. <http://doi.org/10.1016/j.apt.2014.05.017>.
34. Zhang L, Liu B, Zhang Y, Han G, Huang J, Ye J, et al. New perspective on the interface reaction and morphology evolution in the reduction of manganese silicate for silicomanganese alloy production. *Appl Surf Sci*. 2021;539:148210. <http://doi.org/10.1016/j.apsusc.2020.148210>.
35. Pan L, Hu X, Shao B, Li L. Synthesis and high electrocatalytic property of calcium carbonate loaded with silver nanoparticles. *J Sol-Gel Sci Technol*. 2023;108(3):621-9. <http://doi.org/10.1007/s10971-023-06209-4>.
36. Somasundaram K, Rastogi CK, Roy I, Selvin PC, Sudarsan V. Lanthanide ion induced phase decomposition of tetragonal CaWO₄. *Mater Res Bull*. 2019;113:133-40. <http://doi.org/10.1016/j.materresbull.2019.01.027>.
37. Saeed A, Adewuyi SO, Ahmed HAM, Alharbi SR, Al Gami SE, Abolaban F. Electrical and dielectric properties of the natural calcite and quartz. *Silicon*. 2022;14(10):5265-76. <http://doi.org/10.1007/s12633-021-01318-7>.
38. Nedumkallel A. Dielectric studies of nanocrystalline calcium tungstate. *Nanosystems: Phys Chem Math*. 2016;7:599-603.